Low-Speed Wind Tunnel Investigation of a Full-Scale UH-60 Rotor System

Thomas R. Norman
Army/NASA Rotorcraft Division
tnorman@mail.arc.nasa.gov

Patrick M. Shinoda
Army/NASA Rotorcraft Division
US Army Aeroflightdynamics Directorate (AMCOM)
pshinoda@mail.arc.nasa.gov

Cahit Kitaplioglu, Stephen A. Jacklin, and Alex Sheikman
Army/NASA Rotorcraft Division

NASA Ames Research Center, Moffett Field, California

ABSTRACT

An experimental program to test a full-scale UH-60 rotor system in the NASA Ames 80- by 120-Foot Wind Tunnel was completed. The rotor system was installed and tested using a new test stand/facility, the Large Rotor Test Apparatus (LRTA). The experimental program had both operational and research objectives, including 1) demonstration of LRTA capabilities, 2) evaluation of an Individual Blade Control system to reduce vibration and noise, 3) acquisition of low-speed performance and load data for comparison with flight test results and analyses, and 4) validation of a new flow measurement technique. In this paper, the specific objectives and approach for the wind tunnel test are presented along with examples of the research results. Particular attention is placed on describing the experimental program, including the new testing capabilities available with the LRTA.

NOTATION

C_L	Rotor lift coefficient
C_P	Rotor power coefficient
C_T	Rotor thrust coefficient
C_X	Rotor propulsive force coefficient
F_M	Figure of merit
M_{TIP}	Rotor tip Mach number
r	Radial station
R	Rotor radius
α_S	Rotor shaft angle measured from vertical, positive aft, deg
μ	Advance ratio
σ	Rotor solidity

INTRODUCTION

Testing of a full-scale UH-60 rotor system in the NASA Ames 80- by 120-Foot Wind Tunnel was recently completed. The motivation for this testing was based on the objectives of two major programs. The first is a cooperative program between NASA, ZF Luftfahrttechnik GmbH (ZFL), Sikorsky Aircraft Corporation, and the U.S. Army Aeroflightdynamics Directorate to evaluate Individual Blade Control (IBC) technology on noise, vibration and performance. The second is a NASA/Army program to obtain comprehensive measurements of a modern technology rotor for analysis validation and physical understanding.

The ultimate objective of the cooperative IBC program is to demonstrate the technology in flight on a Sikorsky UH-60 helicopter. As a part of the risk reduction effort, it was decided to first test the UH-60 IBC system in both test sections of the National Full-scale Aerodynamic Complex (NFAC) at NASA Ames Research Center. The NFAC includes both the 80- by 120-Foot Wind Tunnel and the 40- by 80-Foot Wind Tunnel. The objective of the 80- by 120- entry was to verify the functionality of the IBC system (integrated with the wind tunnel systems) and to assess the effect of IBC on low-speed noise and vibration. Reference 1 describes (and this paper summarizes) the results of this first test entry. The objective of the planned 40- by 80- entry is to evaluate the ability of IBC to control noise and vibration at all airspeeds and to improve rotor performance.

The objective of the second major program is to obtain comprehensive measurements (including detailed blade pressure measurements) on a current technology rotor (Ref. 2). In particular, the goal is to acquire data in flight and in the wind tunnel as well as equivalent data for a model-scale

Presented at the American Helicopter Society 58th Annual Forum, Montreal, Canada, June 11-13, 2002.

rotor. Testing has been completed for a 1:5.73-scaled UH-60A model rotor in hover (Ref. 3) and in the wind tunnel (Ref. 4), as well as for a full-scale rotor in flight (Ref. 5). The final piece of this program is full-scale wind tunnel testing of the UH-60A in the NFAC. Although the current test in the 80- by 120-Foot Wind Tunnel does not fully meet the goals of the original program (no detailed blade pressure measurements, no high-speed results), it does provide a wealth of data for experimental and analytical comparisons.

In this paper, the UH-60 test program in the 80- by 120-Foot Wind Tunnel is described in detail. Information on test hardware, instrumentation, and data systems is provided. Since this was the first test program to use a new rotor test stand, the Large Rotor Test Apparatus (LRTA), particular emphasis is given to describing its capabilities. Test objectives and approaches are then presented, followed by sample results and discussion.

DESCRIPTION OF THE EXPERIMENT

The test program was conducted in the NASA Ames 80- by 120-Foot Wind Tunnel using a Sikorsky Aircraft UH-60 rotor system mounted on the LRTA. Figure 1 shows the model installed in the wind tunnel. In the following sections, detailed information is provided describing the experiment, including test hardware, instrumentation, data systems, pre-test activities, standard test procedures, and data validation activities.

Figure 1. UH-60 Rotor System installed on the Large Rotor Test Apparatus in the Ames 80-by 120-Foot Wind Tunnel.

Hardware

The wind tunnel, test stand, and all rotating hardware are described in this section. Since this was the first test to use the LRTA, specific emphasis is given to describing its functionality and capability.

NASA Ames 80- by 120-Foot Wind Tunnel

The 80- by 120-Foot Wind Tunnel is part of the NFAC located at NASA Ames Research Center (Fig. 2). The tunnel has an open circuit with a rectangular test section that is 79 ft high, 119 ft wide, and 193 ft long. The maximum test section velocity is approximately 100 knots. The tunnel walls are treated with 6 in of acoustically absorbent material to reduce reflections that can contaminate the noise field. This material provides an absorptivity of greater than 90% down to a frequency of approximately 250 Hz. To reduce contamination by hard surfaces on the test hardware, additional absorptive material was added to selected hard spots on the test section floor.

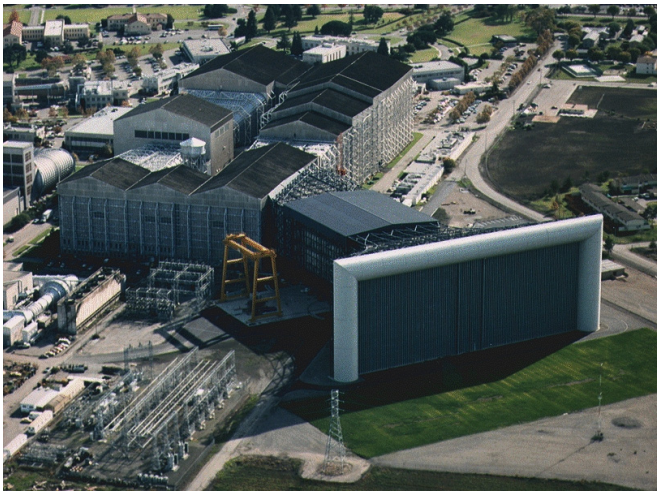

Figure 2. 80-by 120-Foot Wind Tunnel at the National Full-Scale Aerodynamics Complex (NFAC).

LRTA Test Stand

The LRTA (Figs. 1 and 3) is a special-purpose drive and support system designed to test helicopters and tilt rotors in the NFAC. Developed for NASA and the U.S. Army by Dynamic Engineering, Inc., the LRTA is capable of testing rotors at thrust levels up to 52,000 lb. Its primary design features include 1) a drive system powered by two 3000 HP motors, 2) a five-component rotor balance to measure steady and unsteady rotor hub loads, along with an instrumented flex-coupling to measure rotor torque, 3) a six-component fuselage load-cell system to measure steady fuselage loads, 4) a complete rotor control system (including console) with primary and higher harmonic control, and 5) an output shaft

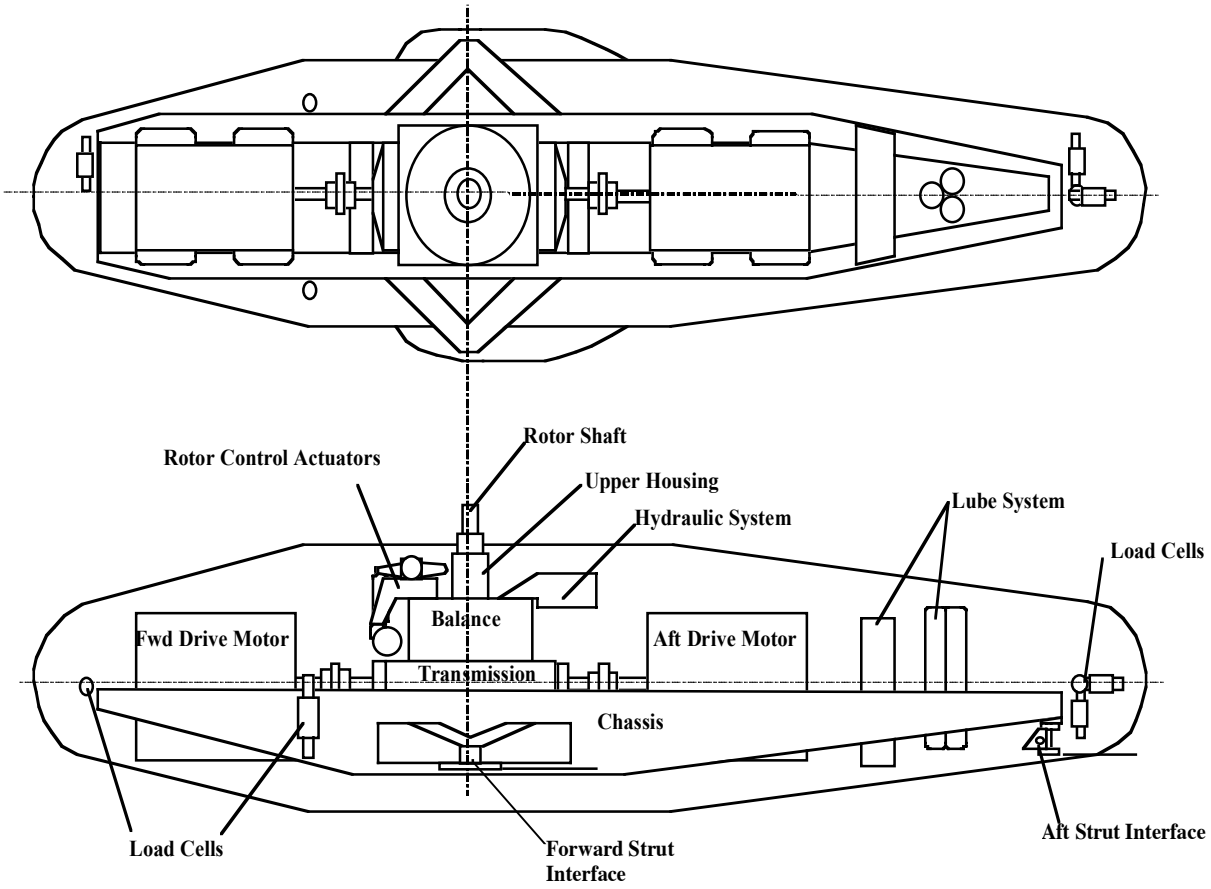

Figure 3. Schematic of the Large Rotor Test Apparatus.

assembly with a replaceable upper shaft for mating with different rotor systems.

The current maximum capabilities of the LRTA (and rotor balance) are provided in Table 1. Note that the maximum resultant hub moment is dependent upon the installed hub height above the balance moment center. Also note that these maximum capabilities represent the limits of the primary LRTA structure, with the exception of the replaceable upper shaft. For most rotor test programs, this upper shaft will have significantly less load-carrying capability than the rest of the LRTA.

Detailed LRTA Description. The LRTA main support chassis (Fig. 3) is designed to mount in the wind tunnel on three struts, two forward and one aft. The length of the aft strut can be adjusted to vary the pitch angle of the apparatus (from 30 deg nose down to 15 deg nose up). The chassis also provides the base to which all LRTA components are attached, including the fuselage fairing, electric drive motors, and transmission.

Table 1. LRTA Capabilities

Parameter	Value
Normal Force	52,000 lb
Shear Force (Resultant)	15,000 lb
Moment (Resultant)	125,000 ft-lb *
Torque	165,000 ft-lb
Rotational Speed	320 RPM
Power	6000 HP
Actuator Loads	5000 ± 6000 lb

* at the balance moment center

The fuselage fairing is basically a body of revolution with an overall length of 480 in and a maximum diameter of 100 in. The fairing structure is connected to the chassis by a statically determinant arrangement of six load cells. These load cells allow determination of the steady aerodynamic forces and moments on the fairing structure.

Two electric motors provide the power to drive the rotor systems on the LRTA. Each motor can provide up to 3000 HP at output speeds ranging from 2390 to 2990 RPM. The motor power is transferred to the rotor shaft by a two-stage transmission. The transmission's 9.329:1 gearbox can provide up to 6000 HP at rotor speeds up to 320 RPM. (Note that the maximum LRTA power is currently limited to 4200 HP by the NFAC power supply).

The LRTA rotor balance, seated on top of the transmission case, is designed to measure both steady and unsteady hub forces and moments. The balance is a large solid ring (49 in diameter) made of a 15-5 PH stainless steel custom forging. Cutouts are made in the center of the ring to leave four symmetrically placed, rectangular flexures. These flexures are designed and gauged to measure five components of forces and moments. These include normal, axial and side forces, together with rotor pitch and roll moments. A sixth component, rotor torque, is measured by an instrumented flexible coupling mounted between the transmission and the rotor shaft. The flexure design is optimized for stiffness to eliminate balance resonances and to provide strain levels adequate for accurate measurement. Temperature stability is provided by circulating cooling water through passages above and below the flexures on both the inside and outside of the balance ring.

The rotor shaft has two distinct sections. The lower section is contained inside the upper housing and is designed to withstand all combinations of LRTA design loads. The upper section extends to the rotor hub and is designed to be replaceable. This universal shaft feature allows accommodation to the requirements of any particular rotor system. Note that this upper section is normally designed to mate with an existing rotor system and, as such, may have significantly less load-carrying capability than the rest of the LRTA. The bottom of the lower shaft connects to the instrumented flexible coupling which, in turn, connects to the transmission. This flexible coupling is designed to measure rotor torque as well as residual thrust.

Rotor control is provided through three identical actuator assemblies, each of which includes both primary and dynamic actuators. These actuator assemblies mount on an actuator plate which, in turn, mounts on the upper housing. The actuator plate was designed to be replaceable to allow for placement of the actuator assemblies at any desired radial or azimuthal location. The primary actuators are high-authority/low-speed ball-screw electric actuators and are used to provide primary control of rotor blade pitch. The primary actuation system can provide up to 11 in of stroke at a maximum rate of 0.335 in/sec. The dynamic actuators are low-authority, high-speed rotary-hydraulic actuators and are used to provide time-varying perturbations to the non-rotating swashplate. This system can provide up to 1.1 in of travel at frequencies up to of 23 Hz. Higher frequency motion is possible for smaller displacements.

Control of the actuator assemblies is provided through two separate, and somewhat independent, position control systems, the Primary Control Console (PCC) and the Dynamic Control Console (DCC). Both of these consoles are pictured in Fig. 4. The PCC provides the operator with static control of the three linear electric (primary) actuators. This position control is achieved by driving three control rod linkages, whose positions define the orientation of the swashplate; and, hence, rotor blade collective and cyclic pitch. In addition to control functions, the PCC also provides numerous displays to give the operator visual feedback of conditions on the test rig, particularly for blade flapping.

Figure 4. LRTA Primary and Dynamic Control Consoles.

The DCC provides the operator with control of the three rotary-hydraulic (dynamic) actuators to provide oscillatory and ramp pitch-angle perturbations about the nominal angle set by the PCC. Internal DCC capabilities allow control inputs to a single actuator or to any of the helicopter's control axes (collective, lateral or longitudinal). Frequencies up to 80 Hz may be input through the DCC for stability estimation or natural frequency investigations. Inputs are also possible at integer harmonics of the main rotor. In addition to these internal capabilities, externally generated signals can be used to drive the dynamic actuators.

Rotating Hardware

The rotating hardware used during this program was predominantly UH-60 flight hardware, with the exception of the instrumentation hat and those components necessary for IBC actuator operation. A schematic of this hardware is shown in Fig. 5 (schematic provided by ZFL). The interface locations between the UH-60 rotor and LRTA occurred at 1) the UH-60 shaft extension, 2) the bottom of the swashplate guide and, and 3) the non-rotating swashplate. The interface locations between the UH-60 rotor and the IBC hardware occurred at 1) the top of the hub, 2) the bottom of the upper pressure plate and, of course, 3) the pitch link locations. The instrumentation hat was mounted on top of the IBC adapter on top of the hub. Details of the rotor, IBC, and instrumentation hat hardware are presented below.

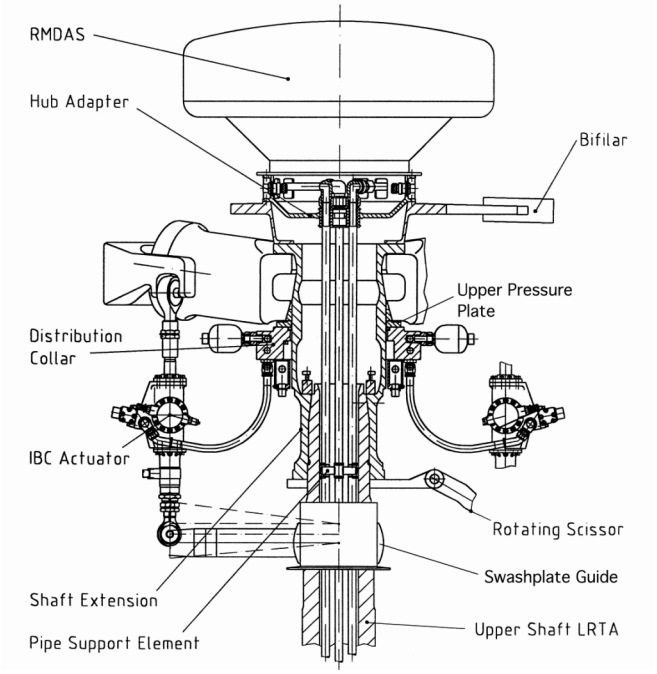

Figure 5. Schematic of rotating hardware.

UH-60 Rotor System. The UH-60 rotor system is a four-bladed, articulated rotor system consisting of four subsystems: hub, blade pitch controls, bifilar vibration absorber, and main rotor blades. Four titanium-spar main rotor blades attach to spindles that are retained in a one-piece titanium hub by elastomeric bearings. These bearings permit the blade to flap, lead and lag. Main rotor dampers are installed between each of the main rotor spindles and the hub to restrain lead and lag motions of the main rotor blades during rotation and to absorb rotor head starting loads. Blade pitch is controlled through adjustable pitch links that are moved by the swashplate. The bifilar vibration absorber is designed to reduce rotor vibration at the rotor head. The absorber is mounted on top of the hub and consists of a four-arm plate with attached weights. For this test program, the bifilar weights were not installed.

The UH-60 rotor blades have a radius of 26.83 ft and nominal chord of 20.9 in, incorporating two related airfoil sections, SC1095 and SC1095 R8, in its design. A summary of these and other main rotor parameters are presented in Table 2 (Ref. 6). The specific blades used in this test program constitute 4 out of the set of 5 matched rotor blades flown during the UH-60 Airloads Program (Ref. 5). Of these five original blades, two were fabricated and heavily instrumented by Sikorsky Aircraft under NASA contract: one with 242 pressure transducers and one with a mix of strain-gages and accelerometers. The heavily pressure-instrumented blade was the one blade not used during this program. Details of the rotor blade instrumentation are provided in a later section.

Table 2. Main Rotor Parameters

Parameter	Value
Number of Blades	4
Radius, ft	26.83
Nominal Chord, in	20.9
Equivalent Blade twist, deg	-18
Blade tip sweep, deg aft	20
Geometric Solidity Ratio	.0826
Airfoil section designation	SC1095/SC1095R8
Thickness, % chord	9.5
100% RPM	258

IBC Hardware. The main rotating IBC components included the IBC actuators, hydraulic distribution collar, and hub adapter. Detailed descriptions of each IBC component can be found in Ref. 7. The hub adapter sat on top of the UH-60 hub-mounted bifilar absorber plate and provided the interface location for the IBC hydraulic and electrical lines coming through the LRTA shaft. The hydraulic distribution collar was attached to the upper pressure plate of the UH-60 rotor head and provided the correct flow and pressure to the IBC actuators as well as a location for installation of hydraulic accumulators and instrumentation enclosures.

The IBC actuators were designed to replace the normally rigid blade pitch links with hydraulic actuators. These four actuators allowed the pitch of each rotor blade to be changed independently of each other and were designed with the capability to impart up to ±6.0 deg at the 2/rev frequency and up to ±1.6 deg at the 7/rev frequency. This large control power was desired to quantify the benefit of large amplitude IBC inputs in the wind tunnel. Reference 7 provides a full discussion of the IBC servo-mechanism, the actuator characteristics, the automatic emergency shutdown feature, the development program, qualification testing, and installation onto the LRTA. The IBC actuators were instrumented with strain gages to measure the axial force

developed in each actuator. These measurements were the equivalent of pitch link forces.

Instrumentation Hat. The instrumentation hat, mounted on top of the IBC hub adapter, provided a location for terminating instrumentation wiring and mounting the Rotor Mounted Data Acquisition System (RMDAS). Details of the RMDAS are provided in the Instrumentation section below. An aerodynamic fairing was designed to protect these components as well as minimize undesirable aerodynamic forces. To reduce later uncertainties when comparing with flight test data, the fairing was designed to duplicate, as closely as possible, the instrumentation fairing used during the UH-60 Airloads program (Ref. 5).

Wind Tunnel Installation

For this test program, the LRTA was mounted on three struts as shown in Fig. 1, allowing a maximum angle-of-attack of ± 15 deg. This installation put the rotor plane (at $\alpha_S = 0$ deg) just above the tunnel centerline (39.8 ft above the acoustically treated floor).

Instrumentation

Approximately 100 parameters were measured on the instrumented rotor blades and hub as outlined in Table 3 and another 149 parameters were measured on the LRTA and in the wind tunnel as shown in Table 4. These two tables include the channel count, the filter type and cut-off frequency, and the sample rate. The following sections will briefly describe these parameter groups.

Table 3. Blade and Hub Rotating Measurements

Measurement Type	Number of gages	Filter Poles*	Filter Cut Off (Hz)	Sample Rate (per rev)
Spindle stress	10	6	167	256
Bifilar arm and spindle	2	8	167	256
Rotating scissors, dampers, shaft bending	6	6	167	256
Hub accelerometers	3	8	167	256
Pitch, flap and lag angles	12	8	167	256
Blade normal, flap, and torsion moments	21	6 or 8	167	256
Blade stress	6	6 or 8	167	256
Blade accelerometers	16	6 or 8	167	256
Blade Pressures	12	6	1670	2048
IBC actuator force	4	6	167	256
IBC actuator positions	8	6	167	256

*All filters are Butterworth

UH-60 Rotor Blade and Hub Instrumentation

The instrumentation on the hub consisted of instrumented spindles, rotating scissors, dampers, and shaft extension for a total of 18 gages. The accelerations of the instrumentation hat (attached to the top of the hub) were measured by 3 orthogonal accelerometers. The hub instrumentation also included specially designed blade motion measurement devices used to determine blade flap, lag, and pitch angles on each blade. These devices were used in the flight test phase of the NASA/Army UH-60A Airloads Program and consisted of 3 transducers for every blade for a total of 12 transducers in the rotating frame. Detailed information on this hardware and on calibration procedures can be found in Ref. 5.

Table 4. LRTA and Wind Tunnel Measurements

Measurement Type	Number of gages	Filter Poles*	Filter Cut Off (Hz)	Sample Rate (per rev)
Balance and Flex-coupling forces and moments	28	5	170	256
Balance and Flex-coupling temps	14	6	1	256
Stationary pushrods, scissors and swashplate guide	8	6	167	256
Control System Positions	12	6	167	256
Model loadcells	6	6	167	256
Model Utilities	54	-	-	-
Tunnel Pressures and temperatures	8	-	-	256
Model angles and RPM	3	-	-	256
Microphones	16	6	1670	2048

*All filters are Butterworth

Two of the four rotor blades carried instrumentation. Blade 1 was the heavily instrumented strain-gage blade used during the Airloads Program, containing 19 strain gages measuring torsion, normal bending, and edgewise bending as well as 16 accelerometers. Blade 3 was instrumented with 3 strain gages at critical locations as back-ups for Blade 1 measurements and also carried 12 pressure transducers. Refer to Fig. 6 for Blade 1 instrumentation locations and Table 5 for the summary of Blade 3 pressure instrumentation.

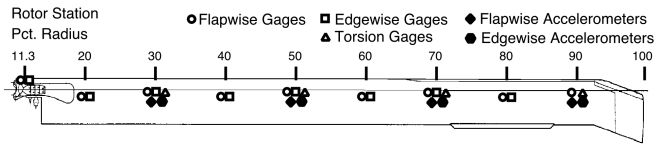

Figure 6. Locations of accelerometers and blade gages on Blade 1.

Table 5. Locations of Pressure Transducers on Blade 3

Surface	Location	
	Radial	Chord
Top	74.10%	4.90%
Bottom	74.10%	4.90%
Top	83.50%	4.90%
Bottom	83.50%	4.90%
Top	86.50%	4.90%
Bottom	86.50%	4.90%
Top	89.50%	4.90%
Bottom	89.50%	4.90%
Top	92.00%	4.90%
Bottom	92.00%	4.90%
Top	96.55%	4.90%
Bottom	96.55%	4.90%

Each of the IBC actuators was instrumented with 2 position transducers and 1 force transducer to facilitate monitoring and control of each actuator (a total of 12 IBC transducers). A more thorough discussion of the function and control of these actuators can be found in Ref. 7.

LRTA Instrumentation

The instrumentation on the LRTA included rotor balance and flex coupling gages, stationary control force and moment gages, fuselage load cells, model utility instrumentation, and control system position transducers.

As discussed earlier, a five-component rotor balance with steady and dynamic load measuring capability is integrated into the LRTA. The four balance flexures are instrumented with 12 primary gages and 12 back-up gages to measure rotor normal, axial and side forces, together with the rotor pitching and rolling moments. In addition, 20 thermocouples are mounted inside the balance to monitor internal balance temperatures and record any temperature gradient present around the circumference or between the metric and non-metric sides of the balance. All of the strain gages and 12 of the rotor balance thermocouples were conditioned and recorded by the data system. In addition, the rotor shaft has an in-line flex-coupling, which is instrumented to redundantly measure rotor torque, residual power-train normal force, and temperature.

An extensive static calibration of the rotor balance was performed prior to the wind tunnel test. For this calibration, the balance was installed in the LRTA and this assembly was positioned in a special calibration test rig (Fig. 7). Hydraulic actuators were used to apply the static calibration loadings. A total of 57 calibration loading sequences were performed for a total of approximately 1100 calibration load points. These data were then analyzed to determine a calibration coefficient matrix to account for interactions. The coefficient matrix could then be used in an iterative scheme to convert the balance measurements to engineering unit data. This method was subsequently used to calculate the balance loading from the calibration voltage data. The errors between the predicted balance loadings and the known applied calibration loadings were calculated. These errors were incorporated into an uncertainty analysis (accounting for both systematic and random errors) to provide an estimate of the overall uncertainty in the balance load measurements. The results of this analysis are shown in Table 6, with the uncertainty being less than 0.25% of the

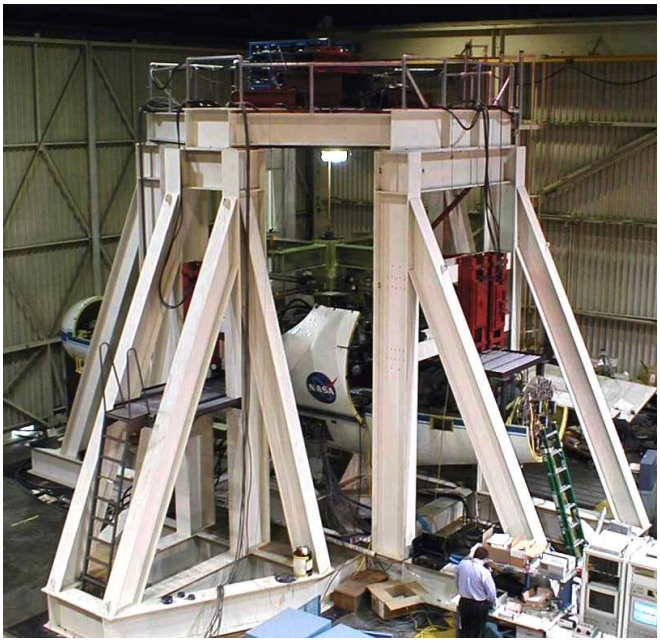

Figure 7. Calibration rig for the LRTA rotor balance.

Table 6. LRTA Balance Accuracy

Parameter	Maximum Cal. Load	Estimated Uncertainty	
		Value	%
Normal Force	30000 lb	60 lb	0.20
Axial Force	15000 lb	20 lb	0.13
Side Force	15000 lb	20 lb	0.13
Pitch Moment	83000 ft-lb	100 ft-lb	0.12
Roll Moment	83000 ft-lb	200 ft-lb	0.24

applied calibration loading for all primary balance components. Detailed information on the balance, including calibration procedures, can be found in Ref. 8.

A total of 8 strain gage measurements were made on stationary control hardware, including three on the stationary pushrods, one on the stationary scissors, and four on the swashplate guide. The LRTA control system also supplied two displacement measurements for every primary actuator and two displacement measurements for every dynamic actuator for a total of 12 measurements.

The LRTA chassis was linked to the aerodynamic fairing with a six-component fuselage load-cell system to measure steady fuselage loads (lift, drag, side, pitch, roll, and yaw). The model was also instrumented with 36 temperature gages, 15 flow and pressure switches, and 3 pressure transducers to monitor the health of various on-board systems.

Wind Tunnel Instrumentation

Eleven standard facility measurements were recorded and used to derive tunnel atmospheric and model operating conditions. These included 8 tunnel pressures and temperatures, 2 model angles, and rotor RPM.

Acoustic Instrumentation

Acoustic data were acquired using 8 microphones mounted on the Acoustic Survey Apparatus (ASA), as well as 8 microphones at fixed positions (Figs. 1 and 8). Microphones 1-8 were mounted on the ASA, a stream-wise traversing mechanism, to probe the acoustic footprint under the advancing side of the rotor where the highest Blade Vortex Interaction (BVI) noise levels would be encountered. Microphones 9-13 were placed forward of the model at positions of estimated high BVI noise, and/or to coincide with similarly positioned microphones during previous tests. Microphone 14 was mounted on the LRTA fuselage and Microphones 15 and 16 were mounted at retreating-side BVI locations. The microphone coordinates are given in Table 7. The coordinate system is centered on the rotor hub when the shaft angle is set to zero ($\alpha_S = 0$ deg).

Instrumentation-grade, 0.5 in condenser microphones were used for the acoustic measurements. The microphone signals were preamplified at the source to minimize signal loss over the long wiring runs. Microphone power supplies provided proper impedance matching. The signals were further amplified to maximize signal-to-noise ratio on the measurement system. An end-to-end calibration of each microphone channel was performed prior to each data run. A fixed frequency piston-phone of known output (nominally 124 dB at 250 Hz) traceable to the NASA Ames Calibration Lab was utilized for the calibrations. These calibrations provided engineering unit conversions that were updated prior to the run.

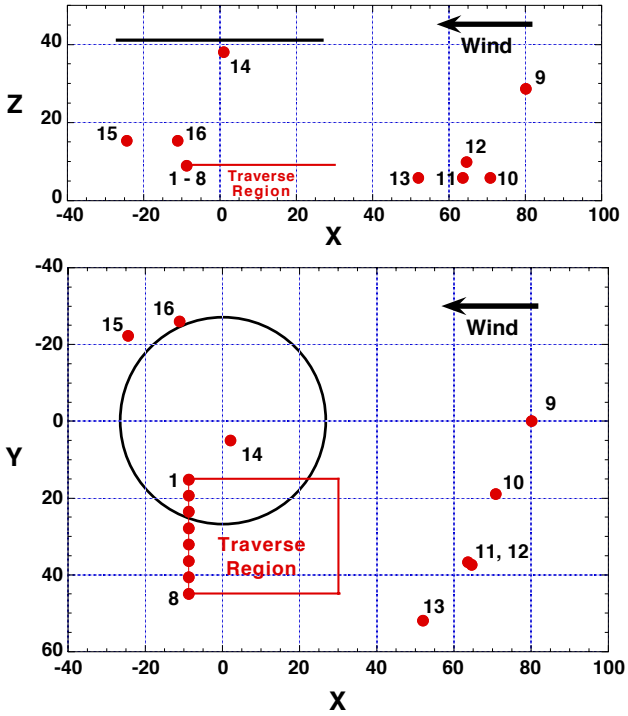

Figure 8. Orientation of microphones and rotor in 80- by 120-Foot test section (dimensions in ft)

Table 7. Microphone Positions

Mic #	x	y	z
1	Trav.	15.13	9.00
2	Trav.	19.38	9.00
3	Trav.	23.63	9.00
4	Trav.	27.88	9.00
5	Trav.	32.13	9.00
6	Trav.	36.38	9.00
7	Trav.	40.63	9.00
8	Trav.	44.88	9.00
9	80.21	0.00	28.73
10	70.91	19.00	5.77
11	63.58	36.71	5.77
12	64.64	37.32	9.84
13	52.60	52.60	5.31
14	2.00	6.10	37.50
15	-24.50	-22.30	15.31
16	-11.10	-26.00	15.31

*All dimensions in feet, origin at rotor hub except z-dimension is height from floor.

Data Acquisition

Three data acquisition systems were used to collect data during this test program. The first system, NFAC Parametric Real-time Information Management Enterprise (NPRIME), a VME-based open-architecture data acquisition system, was located in the facility control room and was used to record high-speed data (2048 samples/rev) and low-speed data (256 samples/rev). The second system, Rotor Mounted Data Acquisition System (RMDAS), was mounted on top of the rotor hub and was used to acquire 64 channels of high-speed data (2048 samples/rev). The third system, Monitoring Front End Data System (MFEDS), was located in the control room and was used to monitor the safety parameters in real time and as an incident recorder. The characteristics of all three systems are briefly described in the following sections.

NPRIME

NPRIME is the primary data acquisition system used in the NFAC. Developed over the past decade (Ref. 9), its design is based on industry-wide standards that allow the use of hardware and software from multiple vendors. The system supports 16-bit static data acquisition (i.e., data that are collected for a specified duration and then averaged to provide statistical results) and dynamic data acquisition (i.e., high-speed data that are collected for a specified duration where all samples are saved). The acquisition can be synchronized to an internal or external clock, or to an external trigger from a spinning rotor.

For this test, NPRIME was configured with two sets of chassis. The first set was configured for low-speed data acquisition and used to record tunnel parameters, stationary measurements on the LRTA and the rotor, all of the safety measurements, and some of the rotating measurements. The second set was configured for high-speed data acquisition and recorded all of the blade pressure parameters and microphone signals.

Thirty-two revolutions of data were digitized and stored at each test condition. The data were digitized at 256 or 2048 samples/revolution (1100 or 8800 samples/sec at a nominal RPM of 258) using the clocking signal from the rotor encoder. All channels were triggered and sampled simultaneously. The anti-aliasing filters were set at a cutoff frequency of 167 or 1670 Hz (Tables 3 and 4).

RMDAS

RMDAS is designed to acquire, digitize, and store rotor-based rotating measurements. The system is mounted on the rotor hub in order to provide the highest quality data by digitizing the transducer signal as close to the transducer as possible. The system consists of 2 circular modules (platters), which are stackable. Each platter supports 64 transducers, providing excitation, filtering, amplification, signal offset, and digitization. The system simultaneously digitizes each input signal at either 1024 or 2048 times per revolution, and supports rotor speeds of between 200 and 550 RPM**.** The 12-bit digitized data on each platter is PCM encoded and sent to the ground station in burst mode at a fixed rate of 17mHz. A summary of RMDAS system capabilities is provided in Table 8.

This test program was the first to use RMDAS for wind tunnel data acquisition. To simplify system checkout, only one platter was used to condition and digitize 64 channels of rotating parameters. To insure proper handling of the signals, two raw analog blade pitch measurements were routed to both RMDAS and NPRIME data systems for data system comparisons.

As with the NPRIME data, 32 revolutions of data were digitized and stored at each test condition. The data were digitized at 2048 samples/revolution using the clocking signal from the rotor encoder. Although all RMDAS channels were triggered and sampled simultaneously, the starting revolution was not necessarily coincident with NPRIME data (they could differ by up to 3 revolutions). The anti-aliasing filters were set at a cutoff frequency of 3000 Hz. All RMDAS data were subsequently filtered digitally at 167 Hz and decimated to 256 samples/revolution prior to transferring to the database.

Table 8. RMDAS System Capabilities

Parameter	Value
Overall system accuracy	1%
DAC	12 bit
Filter	8-pole butterworth low pass (adjustable)
Gain	8-step programmable gain 1,2,5,10,20,50100,500
Input Signal	+/- 5V
Offset	+/- 2.5V
Excitation	Jumper selectable 5,10,12,15 VDC
Calibration	RCAL, VCAL
Balance	Four leg shunt resistor bridge balance

MFEDS

MFEDS is an independent system that serves two basic functions. The first function is the sampling and display of safety parameters as a percentage of the allowable limits. The system provides 16-bit digitization with simultaneous sample and hold of 96 channels at a rate of 2000 samples/second/channel. MFEDS performs real-time display of acquired and reduced data at a rate of 3 times/sec. The data are displayed as bars, representing percentages of user-defined limits, with the capability of changing color when

limits are reached (Ref. 10). The second MFEDS function is the continuous recording of data (up to 3 hours) onto removable media to serve as an incident recorder.

Data Reduction

As discussed above, 32 revolutions of raw digitized data were stored for every measurement acquired with NPRIME or RMDAS. These data were subsequently processed prior to final engineering unit (EU) data storage and/or derived parameter calculation. Different processing was performed for the high-speed acoustic data. Both data reduction schemes are outlined below followed by a description of the derived parameters.

Standard Data Reduction

The data reduction process for all low-speed data is illustrated in Fig. 9. The digital data were initially converted to EU data using standard linear calibration methods. A Fast Fourier Transform (FFT) was then performed on each time history and the resultant data were corrected in the frequency domain for analog filter effects. An inverse FFT was performed on the corrected frequency data, resulting in 32

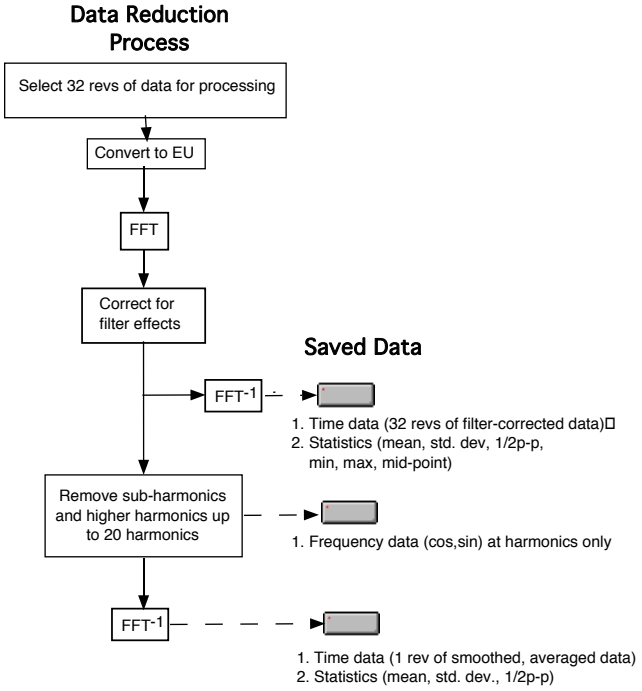

Figure 9. Standard data reduction process.

revolutions of filter-corrected EU data for each measurement. These data, as well as various statistical values, were stored in the database. Additional processing was subsequently performed on the corrected frequency data. All sub-harmonics and higher harmonics above 20/rev were removed from the data and the remaining harmonic frequency coefficients were stored. An inverse FFT was performed on the modified frequency data, resulting in one revolution of "smoothed" data. These data, and the statistics associated with them, were also stored.

Acoustic Data Reduction

Due to both the large amounts of data and to special requirements, the data reduction process for high-speed acoustic data was different. The digital data were initially converted to EU data using the end-to-end calibration procedure described earlier. Preliminary processing of the data was performed after the completion of each run to provide an averaged time history and power spectrum for each microphone. A BVISPL (BVI Sound Pressure Level) acoustic metric, described below, was also calculated and provided guidance for the choice of a test matrix for subsequent data runs.

Initial examination of the data showed excellent rev-to-rev repeatability. Thus, it was determined that a straightforward synchronous average of the data in the time domain, based on the 1/rev trigger, would preserve the pulse-like nature of the BVI events. The subsequent procedure for acoustic data reduction is illustrated in Fig. 10. The 32 revolutions of time history data were synchronously averaged based on the 1/rev trigger pulses, resulting in an averaged time history of one revolution duration of 2048 points. The Fourier transform of this averaged time history yielded a power spectrum with a 1/rev resolution (4.3 Hz for 258 RPM). The averaged time history was bandpass-filtered between the 10^{th} and 50^{th} blade-passage harmonics (172 Hz and 860 Hz, respectively, for 258 RPM), as described in detail in Ref. 11, to focus on the BVI event. Three noise-level metrics were obtained by integrating the respective sound pressure power spectra; OASPL (OverAll Sound Pressure Level) and dBA from the unfiltered spectra and BVISPL from the bandpass-filtered spectra.

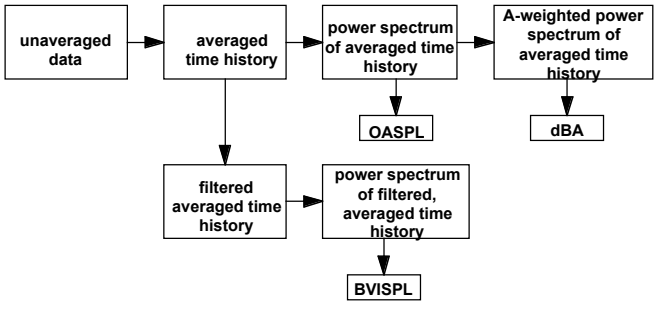

Figure 10. Acoustic data reduction process.

Derived Parameters

The NPRIME data reduction software allows for the calculation of many derived parameters. For this test

program, over 500 interim and final derived parameters were calculated for every data point acquired. Examples of derived data include tunnel velocity, rotor balance and fuselage forces and moments, blade motion angles, rotor control positions, and various IBC parameters. These derived data also include all non-dimensional parameters, including rotor coefficients for thrust and power, advance ratio, and tip Mach number.

Pretest Activities

Prior to blades-on research testing, a number of pretest activities were performed, including shake testing, tare data acquisition, and track and balancing. This section provides details of these activities.

Shake Testing

A shake test of the LRTA was conducted immediately following installation in the 80- by 120-Foot Wind Tunnel. This test provided the resonant frequencies and hub impedances necessary to complete a ground resonance analysis. Accelerometer response data were acquired for both lateral and longitudinal inputs at the hub for a number of different wind tunnel scale configurations (scales locked, scale dampers on, and scale dampers off). These results were used in conjunction with UH-60 blade damper models to verify that the rotor/LRTA was stable in both hover and forward flight.

During the shake test, data were also acquired to evaluate the dynamic characteristics of the rotor balance. Although these data were not sufficient for a complete dynamic calibration of the balance (Refs. 12-14), they did provide an indication of balance characteristics. Figure 11 shows the frequency response function of balance side force due to side force loading at the hub. Figure 12 shows the frequency response function of balance axial force due to axial force loading at

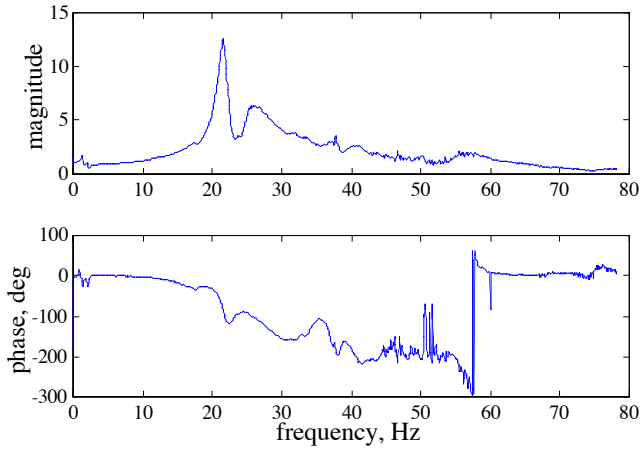

Figure 11. Balance side force response due to hub side force input.

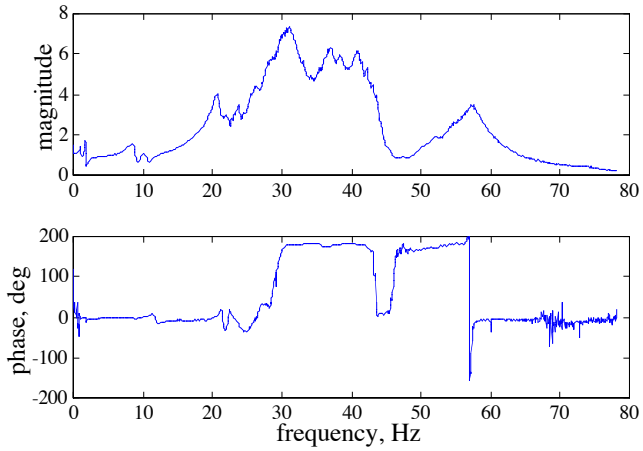

Figure 12. Balance axial force response due to hub axial force input.

the hub. These results suggest that there is little shear force amplification at frequencies below 2/rev (8.6 Hz), but that amplifications do exist at higher frequencies, especially near 21 Hz. These results also indicate that the balance characteristics are relatively smooth and a complete dynamic calibration should provide excellent dynamic hub load results. Table 9 presents the frequency response magnitude and phase for the 1/rev and 4/rev frequencies of this rotor (4.3 and 17.2 Hz).

Table 9. Frequency Response of Balance in Side and Axial Directions

Direction	Frequency	Magnitude ratio	Phase deg
Side Force	1/rev	0.90	0
	4/rev	2.85	-30
Axial Force	1/rev	0.93	-3
	4/rev	1.87	-8

Tares

Tare data were acquired to compensate for both gravity effects and hub aerodynamic interference. The effect of gravity, or weight tare, was determined by acquiring mean rotor balance and fuselage load cell data as a function of model angle-of-attack, both with and without rotor blades installed. The effect of hub aerodynamics was determined by acquiring mean wind-on balance data without the rotor blades installed. These aerodynamic tare data were acquired with hub rotation over the complete range of tunnel speeds and model angles tested. The resultant data were subsequently analyzed to provide smooth analytical functions as a function of model angle-of-attack and wind tunnel dynamic pressure. The weight and aerodynamic tare functions were then calculated on a point-by-point basis and subtracted from the acquired data to isolate the measurements of interest.

Track and Balance

As done for all rotor systems, whether in flight or in the wind tunnel, the instrumented UH-60 rotor was adjusted to achieve proper track and balance characteristics. Weights were applied at the hub to minimize the 1/rev shear force as measured by the rotor balance. Blade tracking was accomplished by adjusting pitch link lengths so that all four blades flew in the same plane (± 0.5 blade-tip thickness at an azimuth angle of 240 deg). These adjustments were made in hover and verified at 60 knots.

Standard Test Procedures

In this section the standard test procedures are described, including the methods used to trim the rotor and the types of data to be acquired in a typical run.

Trim Procedures

Two different trim procedures were used during this test program. The first was used when trying to match aircraft flight conditions and for IBC vibration testing. The second was used for parametric studies and BVI noise testing.

For direct performance and load comparisons with flight test results, C_L/σ, M_{TIP}, μ, α_S, and pitching and rolling moments were all set to match flight test conditions. Pitching moment and shaft angle were varied at these specified conditions to determine their sensitivity on measured loads. For IBC vibration testing, these same parameters were set to match flight test conditions. When IBC inputs were introduced, the rotor was re-trimmed in order to hold lift, propulsive force and hub moment constant. This was accomplished by adjusting shaft angle, collective pitch angle, and lateral-longitudinal cyclic pitch angles.

For performance and load comparisons with predictions as well as for BVI noise testing (with and without IBC), C_T/σ, M_{TIP}, μ, and α_S were set to the desired test condition. Cyclic pitch was then adjusted to minimize the first harmonic flapping (± 0.4 deg). For this case, the rotor tip-path-plane angle-of-attack and the rotor shaft angle were essentially equal.

Standard Data

Under normal situations, each run contained a beginning and ending non-rotating reference point, a beginning and ending hover reference point (4 deg collective, α_S=0 deg, and M_{TIP}=0.650) and when possible, a beginning forward flight reference point (C_T/σ=0.08, α_S=0 deg, M_{TIP}=0.650, μ=0.150). These reference points were used during the run as well as post-run to help validate data quality and repeatability.

Data Validation

A number of approaches were used both during and after the test program to validate the acquired data. These approaches included simple instrumentation checks, internal consistency checks (comparing one type of measurement with another), and external consistency checks (comparing results with predictions and other experiments). Examples of some of these approaches are described in this section. Although these approaches have been applied to a considerable portion of the database, complete validation of the data has not yet been completed.

Instrumentation Checks

Standard instrumentation checks, such as resistor-shunts of each strain gage, were the primary method for identifying faulty measurements. These checks included acquiring both a zero point and a shunt point at the beginning and end of every run. The zero point data were used to identify measurements with large drifts and the shunt point data were used to ensure the gages were functioning properly. The end points were compared with the beginning points to verify that no problems occurred during the run.

Internal Consistency Checks

A number of internal consistency checks were performed on the test data. One straightforward check was the comparison of measurements which have redundant gages located on the same hardware. The most obvious examples for this test were the rotor balance measurements. Since these were critical measurements, direct comparisons were made between the primary and backup balance components on a daily basis. Figure 13 is an example of this type of comparison, showing the averaged time histories of primary and backup axial force.

A second consistency check was the comparison of different revolutions of the same measurement. For steady, forward-flight testing, these different revolutions should ideally show little variation. Figure 14 is an example of this type of comparison, showing all the revs for a single point for one of the pitch link measurements.

A third consistency check was the comparison of similar measurements made on different hardware. One example for this test was the root edgewise bending loads, with separate instrumentation on each of two blades. Figure 15 provides an example of this type of comparison, showing the averaged time histories of each bending load.

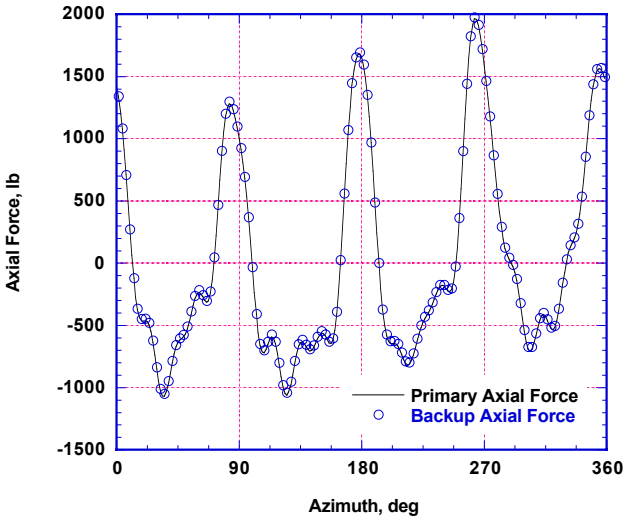

Figure 13. Comparison of primary and backup axial force as a function of blade azimuth for a single point (μ=0.150, M_{TIP}=0.650, C_T/σ=0.08, α_S=0 deg).

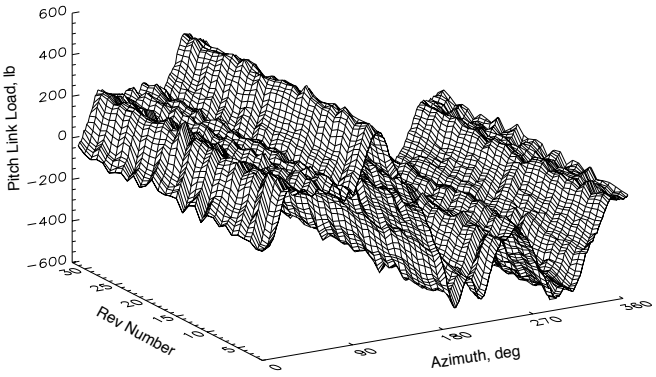

Figure 14. Pitch link load as a function of blade azimuth and rev number (μ=0.175, M_{TIP}=0.650, C_T/σ=0.09, α_S=7 deg).

A final consistency check was the comparison of the same measurement at several repeat points, both during the same run and between runs. This check helped evaluate both data and set point repeatability. Figure 16 provides an example of this type of comparison.

External Consistency Checks

Whenever possible, data were compared to predictions and to other experimental data. For instance, rotor performance measurements were routinely compared with pre-test predictions both during and after each run. These comparisons would ensure that the data followed the expected trends and, if not, that the difference was understood. Specific examples of these types of comparisons can be found in Ref. 15.

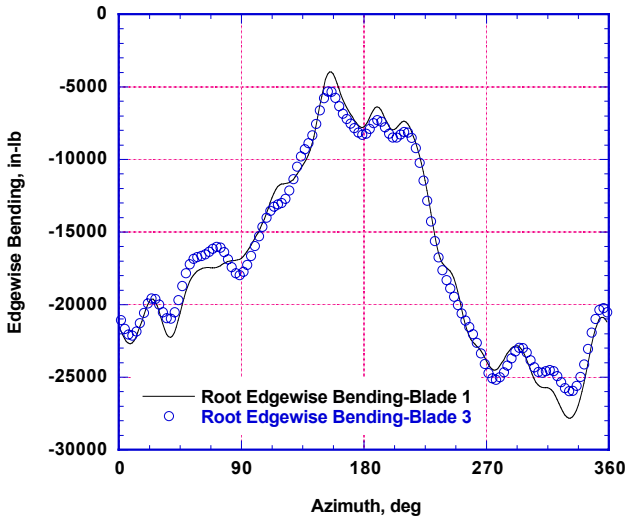

Figure 15. Comparison of root edgewise bending moments on two blades as a function of blade azimuth for a single point (μ=0.150, M_{TIP}=0.650, C_T/σ=0.08, α_S=0 deg).

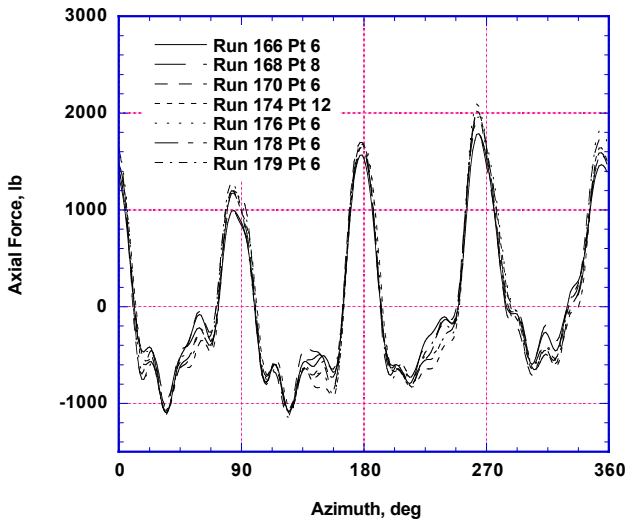

Figure 16. Comparison of primary axial force as a function of blade azimuth for multiple reference (μ=0.150, M_{TIP}=0.650, C_T/σ=0.08, α_S=0 deg).

TEST OBJECTIVES AND APPROACH

As mentioned earlier, this test program had both operational and research objectives. In the following section, each of these objectives is presented along with a discussion of the test approach used.

The operational objective was to demonstrate the LRTA's capabilities and limitations for testing large-scale rotors in the NFAC. This included the evaluation of the LRTA and

facility utilities (including motors and transmission), the rotor control system and console, and the rotor and fuselage balance systems. This objective was met through lengthy subsystem testing as well as wind-on rotor testing.

The primary research objective was to evaluate the potential of a new IBC system to reduce helicopter noise and vibration. To accomplish this, the standard UH-60 pitch links were replaced by servohydraulic actuators designed and manufactured by ZFL (Ref. 7). The effects of IBC on noise and vibration were determined at two different operating conditions by varying the IBC frequency, amplitude, and phase.

The main acoustic objective was to establish the BVI noise characteristics of the baseline UH-60 rotor, specifically to establish the operating conditions for maximum BVI noise. Subsequently, it was desired to establish the amount by which the maximum BVI noise could be reduced with the application of IBC.

The main performance and loads objective was to provide low-speed validation data for comparison with flight test and analytical results. Testing included 1) speed sweeps at specific thrusts and rotor shaft angles, and 2) thrust sweeps at specific tunnel velocities and rotor shaft angles. To correlate with flight test results, specific test points corresponding to known flight test conditions were acquired.

The final objective was to evaluate the capability of the Planar Doppler Velocimetry (PDV) technique to accurately measure flow velocities in large-scale, vortical flows. This relatively new technique provides a potential alternative to flow velocity measurements in the NFAC (Ref. 16). Data were acquired at three speeds without the rotor installed and at one speed and three thrust conditions with the rotor installed. A schematic of the PDV setup is shown in Fig. 17.

To accomplish these objectives, data were acquired over a wide range of thrust, speed, and shaft angles (at M_{TIP}=0.650). A summary of these conditions as a function of research objective is presented in Table 10. During the course of this program, over 1000 forward-flight data points were acquired. This total does not include data acquired during hover, weight and aerodynamic tares, and LRTA sub-system checkouts.

SAMPLE RESULTS AND DISCUSSION

In this section, sample results and discussion are provided for each of the primary test objectives. Detailed results can be found in Refs. 1, 15, 17, and 19.

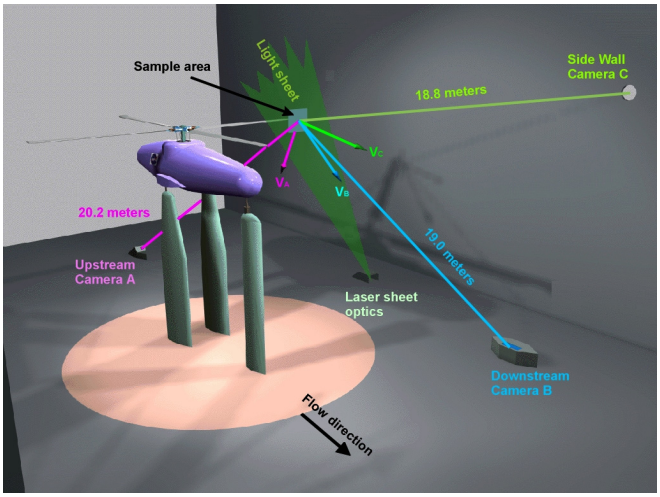

Figure 17. Schematic of PDV installation in the 80- by 120-Foot Wind Tunnel.

Table 10. Nominal Test Envelope

Objective	α_S, deg	C_T/σ	μ
IBC	4, 7	.09	.175
	-.69, -3	.073	.11
		(16,800 lb)	(46 knots)
Acoustics	-6 to 10	.09	.125 to .19
	4, 7	.09	.175
Speed Sweep	0	.06, .08, .09	0 to .19
	-5	.09	0 to .19
Thrust Sweep	-10	.02 to .095	.05, .10, .15, .175, .19
	-5	.02 to .11	.05, .10, .15, .175, .19
	0	.02 to .115	.05, .10, .15, .175, .19
	5	.02 to .115	.05, .10, .15, .175, .19
	7.5	.02 to .115	.175
	10	.03 to .095	.10
Flight Test Correlation	0, -1.5, -3	.08	.091, .110, .129, .149, .178
	-.5, 4	.08	.057
PDV	0	.06, .08, .10	.15

* All data were acquired at M_{TIP} = 0.650

LRTA Operations

Since this was the first test program to utilize the LRTA, considerable effort was taken to verify its capabilities. This effort included integration with wind tunnel subsystems (motor power, cooling water, hydraulic supply) as well as verification of internal systems (lubrication system, rotor balance, rotor control system). Significant attention was given to improving the lubrication system (to allow full angle-of-attack) and to identifying the startup procedures necessary for accurate and repeatable balance measurements. Ultimately, all wind tunnel and LRTA systems worked well, allowing for the successful completion of this test program and demonstrating the general utility of the LRTA for large-scale rotor testing in the NFAC.

Individual Blade Control

The effects of IBC on vibration and noise were evaluated at a limited number of test conditions (Table 10). This evaluation required input of individual IBC actuator displacements at various frequencies, magnitudes, and phase angles. An example of the direct effect of these inputs on blade pitch can be seen in Fig. 18 for two different magnitudes of 2/rev input. These results demonstrate that 1) the IBC actuators were providing the correct inputs to achieve the desired pitch variations and 2) these pitch variations could be large compared to those necessary for 1/rev trim.

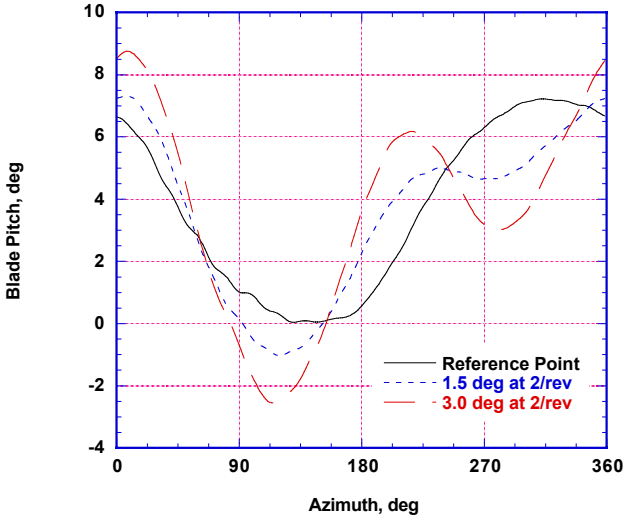

Figure 18. The effect of 2/rev IBC input on blade pitch measurements (μ=0.175, M_{TIP}=0.650, C_T/σ=0.09, α_S=7 deg).

Although the IBC test envelope was limited, sufficient data were acquired to verify the beneficial effect of IBC on UH-60 vibration and noise. Total vibratory hub load reductions of approximately 70% were achieved applying IBC at low-speed, forward-flight test conditions. At test conditions simulating descent flight typical of noisy landings, IBC produced large noise reductions. Although the average BVI noise reduction was between 8-10 dB, at some locations the noise was reduced by as much as 12 dB. A complete description of these and other IBC results can be found in Ref. 1.

Acoustics

To establish the operating conditions for maximum BVI noise (up to μ=0.190), acoustic data were acquired while systematically varying the rotor operating parameters (including C_T/σ, α_S, and μ). Figure 19 is a summary of the results for one of the forward microphones, showing the variation of BVI noise with shaft angle at fixed M_{TIP} and C_T/σ for several advance ratios. The BVI noise peaked at a nose-up angle near 5 deg for all advance ratios. Also, it can be seen that the BVI noise level is much less sensitive to advance ratio, over the range tested, than to shaft angle.

After establishing the peak BVI noise conditions, the acoustic footprint under the advancing side of the rotor was obtained using the microphone traverse. An example is shown in Fig. 20 for one high BVI case. Similar footprint data were obtained for other high BVI conditions.

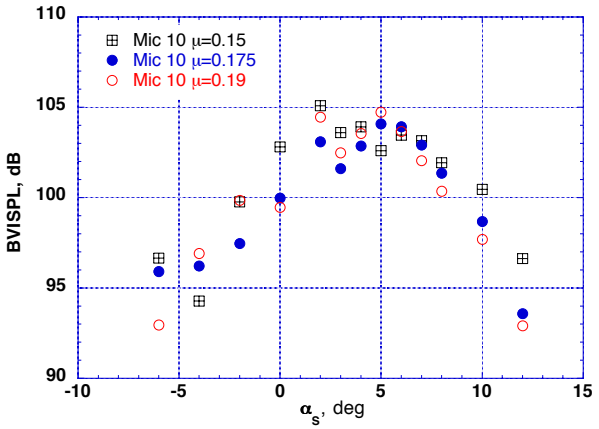

Figure 19. BVI noise variations as a function of shaft angle and advance ratio (M_{TIP}=0.650, C_T/σ=0.09).

The influence of IBC on BVI noise was then investigated by systematically varying the IBC inputs of frequency, phase, and amplitude at one of the high BVI noise conditions. Results of the IBC investigation are discussed above and in Ref. 1.

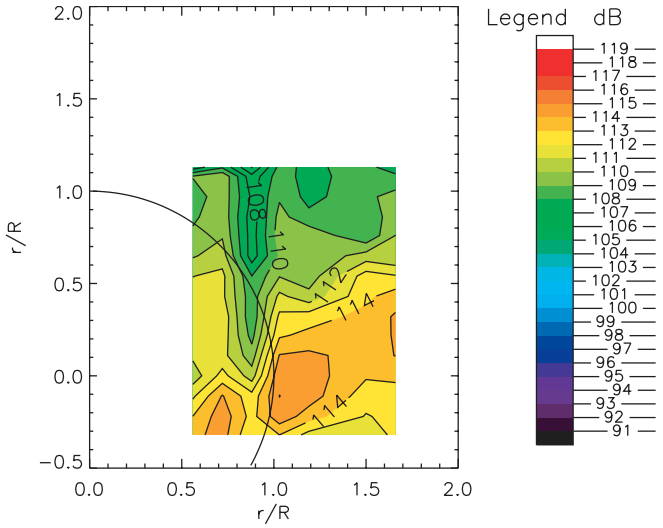

Figure 20. Acoustic footprint under advancing side of rotor (μ=0.190, M_{TIP}=0.650, C_T/σ=0.09, α_S=7 deg).

Performance and Loads

Performance and load data were acquired to evaluate the potential of the wind tunnel for hover testing and to provide low-speed full-scale validation data for comparison with analyses, full-scale flight, and small-scale wind tunnel tests. Sample results are presented in this section. Detailed results can be found in Refs. 15 and 17.

Hover

In order to evaluate the effects of the wind tunnel walls on hover performance results, data were acquired at 4 different shaft angles (α_S =-15, -7.5, 0, 7.5). The assumption was that at higher shaft angles (plus or minus) the effect of the walls would be minimized, with the rotor wake convected down the tunnel rather than recirculated. The data indicate that differences in hover figure of merit do exist as a function of shaft angle, especially at α_S =0 (Fig. 21).

These data were ultimately compared to data from three different flight tests and three different small-scale wind tunnel tests. After appropriate corrections to the flight test data were made (converting engine power to shaft power and accounting for download), the final hover comparisons are shown in Fig. 22. Although there is limited overlap in the data, the trends indicate reasonable consistency between the different test programs, with the DNW test appearing a little higher and the full-scale wind tunnel test appearing a little lower than the other data. Additional details and discussion can be found in Ref. 15.

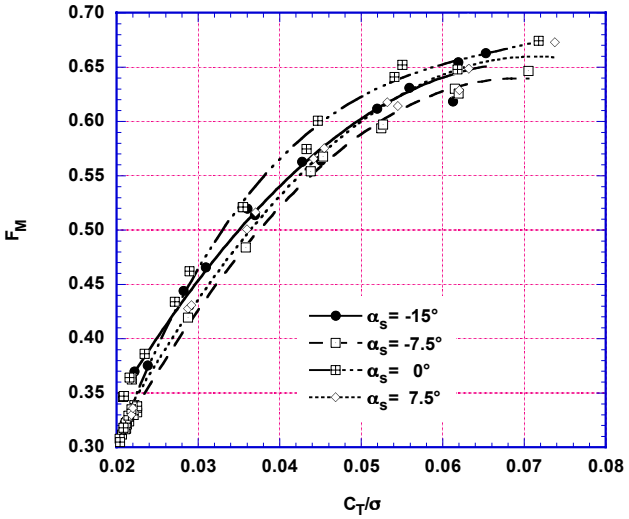

Figure 21. Effect of shaft angle on rotor figure of merit, M_{TIP}= 0.650.

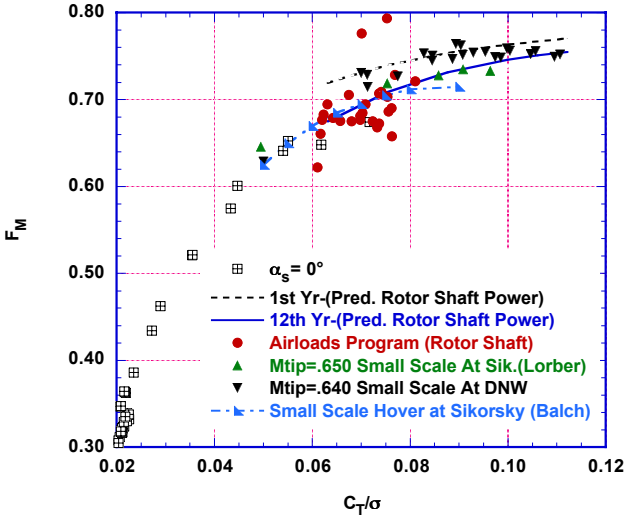

Figure 22. Comparison of rotor figure of merit from four experiments in three facilities and three flight tests. Figure from Ref. 15.

Forward Flight

Numerous speed and thrust sweeps were conducted (Table 10) to generate the forward flight data necessary for correlation with analyses and other test programs. Sample data for an advance ratio of 0.150 are presented in Figs. 23 and 24. Analytical results using CAMRAD II (Ref. 18) are also shown for comparison. Details of these analytical comparisons as well as comparisons with small-scale wind tunnel results are presented in Ref. 15.

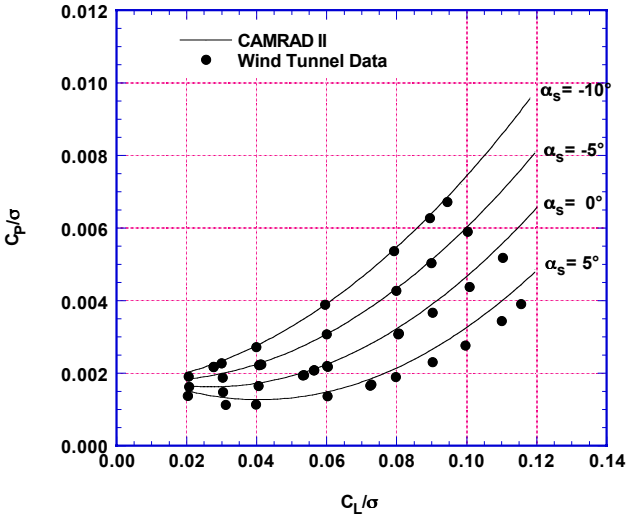

Figure 23. Measured and calculated rotor power vs. rotor lift for various rotor shaft angles at μ=0.150, M_{TIP}=0.650.

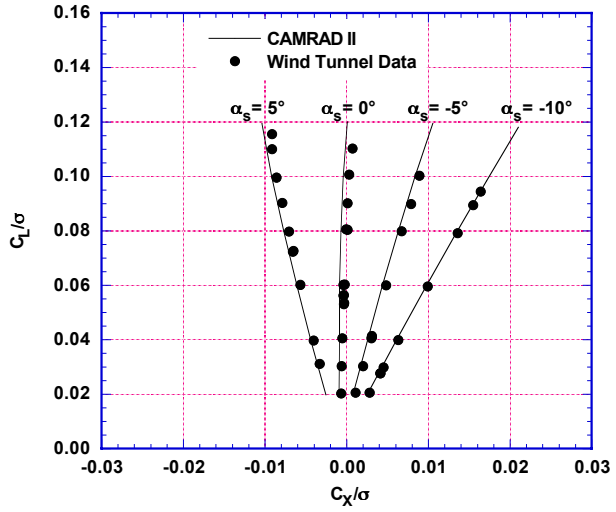

Figure 24. Measured and calculated rotor propulsive force vs. rotor lift for various rotor shaft at μ=0.150, M_{TIP}=0.650.

A direct comparison of rotor loads with flight test results was performed for a limited number of conditions in Ref. 17. For these cases, the rotor was trimmed to match the thrust and moments measured in flight. Sample results comparing the oscillatory flap bending moments for three radial stations at one flight condition are presented in Fig. 25. In general, there is good agreement between the flight and wind tunnel results for this condition. Similar agreement was found at

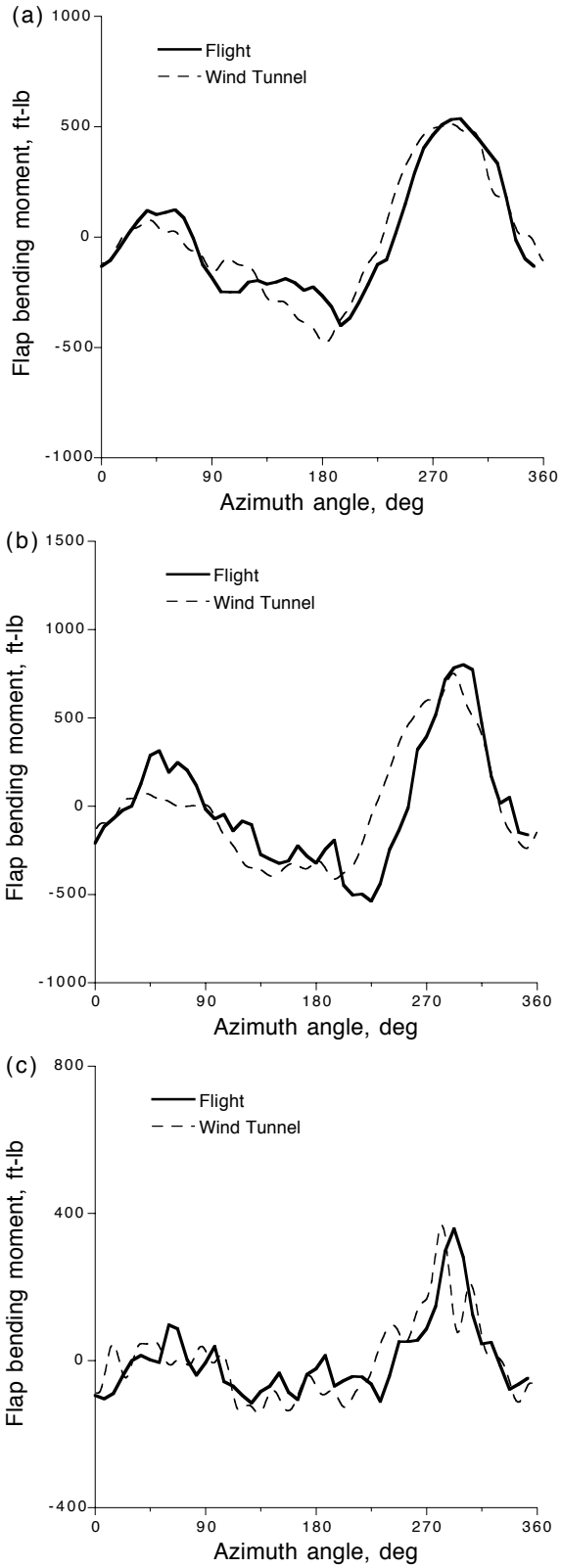

Figure 25. Comparison between flight and wind tunnel tests of oscillatory flap bending moments at (a) r/R=0.5, (b) r/R=0.7, (c) r/R=0.9, (μ=0.178, C_T/σ=0.08).

other radial stations and forward speeds. These results validate the use of full-scale wind tunnel testing to simulate flight for these types of measurements.

Planar Doppler Velocimetry (PDV)

The primary purpose of the PDV testing was to address the implementation issues identified in an earlier test program (Ref. 16) and validate the technique for large-scale rotor tests by acquiring three-dimensional velocity vector fields of UH-60 rotor tip vortices. A summary of the results is provided below; complete details can be found in Ref. 19.

Figure 17 is a schematic of the PDV components in the wind tunnel and includes the optical path lengths from each camera to the sample area. A detailed discussion of the function of each of these components can be found in Refs. 16 and 19. The resultant sample area of approximately 5 ft-square was centered near the blade tip at an azimuth angle of 90 degrees.

Flow field measurements were made with and without the rotor. Undisturbed flow measurements without the rotor were made for free-stream velocities of 30, 60, and 80 knots. The best results came at the two higher speeds, showing a uniform velocity field with the spatially-averaged total velocity within 4-6% of that measured by the wind tunnel systems. Overall, these results showed that the PDV measurements provided flow-field definition with sufficient accuracy to characterize the flow.

With the rotor installed, blade wake measurements were made for one thrust condition (C_T/σ=0.08) at five different wake ages (15, 30, 45, 60, and 75 deg behind the blade) and for one wake age (15 deg) at three thrusts (C_T/σ=0.06, 0.08, 0.10). Figures 26 and 27 show examples of the final phase-averaged results for one condition. Figure 26 is a contour plot of the normalized axial velocity. The cross indicates rotor blade tip position as it passes through the light sheet and the localized region just above and inboard of the blade tip is the primary vortex core. Figure 27 shows the normalized axial and vertical velocity profiles through the primary vortex. The results in Fig. 26 also demonstrate some of the problems encountered during this portion of the testing. In particular, due in part to other testing priorities limiting PDV efforts, the light sheet was partially misaligned with the field of view throughout these PDV measurements. This misalignment, in conjunction with some seeding problems, reduced the size of the useful measurement area. This can be seen in Fig. 26, as data are available in only a portion of the original measurement area.

Unfortunately, for some of the conditions/wake ages tested, the primary vortex was outside or near the edge of this reduced measurement area, thereby compromising the vortex velocity data. It was possible, however, to identify vortex core locations for most of the conditions tested. Figure 28 is a summary plot of these core locations as a function of thrust and wake age. The base points at zero degrees for each thrust are the coordinates where the blade tip passes through the light sheet. These results show that as the thrust is increased and the wake ages, the primary vortex moves further inboard and above the rotor hub.

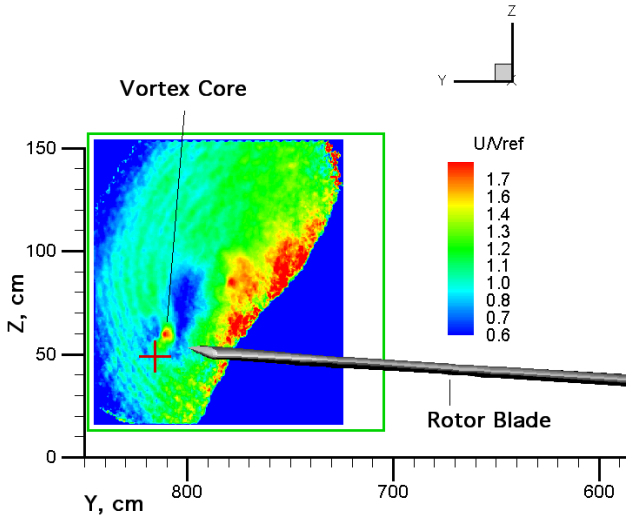

Figure 26. Normalized axial velocity field contour at 90 deg azimuth angle, looking downstream (μ=0.150, M_{TIP}=0.650, C_T/σ=0.08, α_S=0 deg, 15 deg wake age).

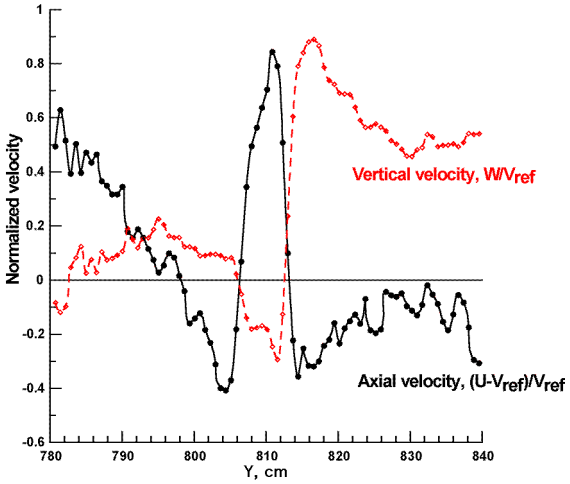

Figure 27. Normalized axial and vertical velocity profiles through the primary tip vortex core, looking downstream (μ=0.150, M_{TIP}=0.650, C_T/σ=0.08, α_S=0 deg, 15 deg wake age).

Although some improvements in the technique are desirable (better seeding, intensified cameras), the results from this test program indicate that the PDV concept for measuring flow-field velocities in large facilities is viable. In particular, its ability to measure rotor vortex wake velocities over long

distances provides a reasonable alternative to other flow measurement techniques.

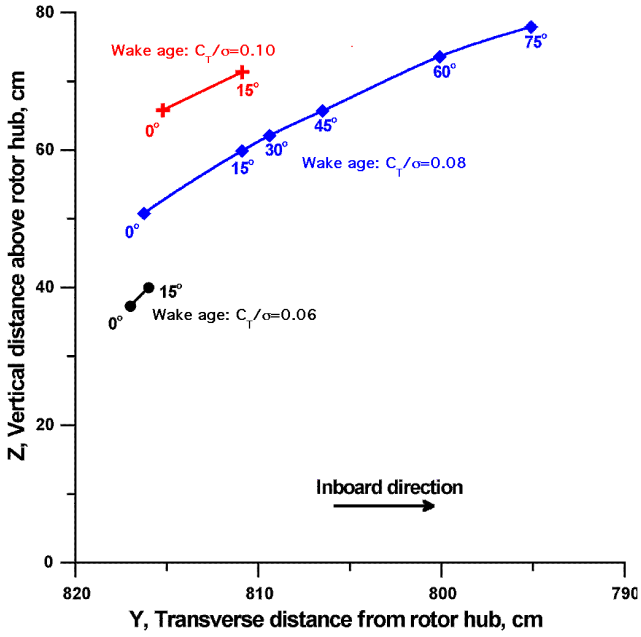

Figure 28. Observed primary vortex locations for various thrusts and wake age (μ=0.150, M_{TIP}=0.650, α_s=0 deg, 90 deg azimuth).

CONCLUDING REMARKS

An experimental program to test a full-scale UH-60 rotor system in the NASA Ames 80- by 120-Foot Wind Tunnel has been completed. The rotor system was installed and tested using a new test stand/facility, the Large Rotor Test Apparatus (LRTA). The following conclusions can be reached as a result of this program:

1) The LRTA provides an excellent means for testing large-scale rotors in the NFAC. The load capacity, control system capabilities, and rotor balance measurement accuracy were all verified during this program.

2) IBC actuators were successfully integrated with the UH-60 and the LRTA to evaluate their effect on noise and vibration. Limited low-speed testing demonstrated that BVI noise reductions up to 8-12 dB and overall vibratory hub load reductions of 70% were possible.

3) BVI acoustic data were acquired to identify the peak BVI noise conditions and provide a baseline for IBC testing. It was found that the BVI noise levels were much less sensitive to advance ratio than shaft angle.

4) Hover performance measurements showed a measurable difference due to shaft angle, especially at α_s=0. Comparisons with flight and small-scale wind tunnel data indicated reasonable consistency between the different test programs, with the full-scale wind tunnel data appearing slightly lower than the rest.

5) The forward flight portion of this program provided high quality data for analysis validation of rotor performance and loads. Limited comparisons with flight test results showed favorable agreement.

6) Planar Doppler Velocimetry was shown to be a viable technique for measuring flow-field velocities in large facilities, including those in the rotor wake.

ACKNOWLEDGEMENTS

The authors would like to acknowledge the significant efforts of NASA's LRTA/UH-60 test team in preparing the model, finding and fixing problems, and performing the day to day operations necessary to have a successful program. Special acknowledgement is made to the program's test managers, Al Lizak and Mark McGlaughlin, for their expertise and dedication. We would also like to acknowledge the efforts of Dr. Robert McKenzie and Mike Reinath, without whom the PDV flow-field measurements would not have been possible. Finally, we are grateful to NASA's partners in the IBC test program, ZFL and Sikorsky, for their valuable expertise and support during all phases of the test.

REFERENCES

1. Jacklin, S.A., Haber, A., deSimone, G, Norman, T.R., Kitaplioglu, C., Shinoda, P., "Full-Scale Wind Tunnel Test of an Individual Blade Control System for a UH-60 Helicopter," American Helicopter Society 58th Annual Forum, Montreal, Canada, June 2002.

2. Watts, M. E., and Cross, J. L., "The NASA Modern Technology Rotors Program," AIAA 3d Flight Test Conference, April 1986.

3. Lorber, P. F., Stauter, R. C., and Landgrebe, A. J., "A Comprehensive Hover Test of the Airloads and Airflow of an Extensively Instrumented Model Helicopter Rotor," American Helicopter Society 45th Annual Forum, May 1989.

4. Lorber, P. F., "Aerodynamic Results of a Pressure-Instrumented Model Rotor Test at the DNW," *Journal of the American Helicopter Society*, Vol. 36, No. 4, October 1991.

5. Kufeld, R.M., Balough, D.L., Cross, J.L., Studebaker, K.F., Jennison, C.D., and Bousman, W.G., "Flight

Testing of the UH-60A Airloads Aircraft," American Helicopter Society 50th Annual Forum, Washington D.C., May 1994.

6. Buckanin, R. M., Gould, W., Losier, P. W., Downey, D. A., Lockwood, R., Webre, J. L., Hagan, J. F., Cason, R. W., and Yourn, C. J., "Rotor Systems Evaluation, Phase I," AEFA Project No. 85-15, March 1988.

7. Haber, A.; Jacklin, S.A.; and deSimone, G., "Development, Manufacturing, and Component Testing of an Individual Blade Control System for a UH-60 Helicopter Rotor," American Helicopter Society Aerodynamics, Acoustics, and Test and Evaluation Technical Specialists Meeting, San Francisco, CA, January 2002.

8. van Aken, J. M., Shinoda, P. M. and Haddad, F., "Development of a Calibration Rig for a Large Multi-Component Rotor Balance," 46th International Instrumentation Symposium of the Instrument Society of America, Bellevue, WA, May 2000.

9. Liu, M., "A VME Based Open Architecture Data Acquisition System," Presented at the 42nd International Instrumentation Symposium, San Diego, CA, May 1996.

10. Liu, M., Osaki, R., "A VME Based Safety of Flight Monitoring System," Presented at the 43rd International Instrumentation Symposium, Orlando, FL, May 1997.

11. Kitaplioglu, C., "Blade-Vortex Interaction Noise of a Full-Scale XV-15 Rotor Tested in the NASA Ames 80- by 120-Foot Wind Tunnel," NASA Technical Memorandum TM-1999-208789, July 1999.

12. van Aken, J. M., Peterson, R. L., and Freedman, C. J., "Calibration Results of the NASA Ames Rotor Test Apparatus Steady/Dynamic Rotor Balance," American Helicopter Society Aeromechanics Specialists Conference, San Francisco, CA, January 1994.

13. Wang, J. M., and van Aken, J. M., "Correlation of Vibratory Hub Loads for a Sikorsky Full-Scale Bearingless Main Rotor," American Helicopter Society 50th Annual Forum, Washington D.C., May 1994.

14. Peterson, R. L. and van Aken, J. M., "Dynamic Calibration of the NASA Ames Rotor Test Apparatus Steady/Dynamic Rotor Balance," NASA TM 110393, April 1996.

15. Shinoda, P., Yeo, H., Norman, T.R., "Rotor Performance of a UH-60 Rotor System in the NASA Ames 80- by 120-Foot Wind Tunnel," American Helicopter Society 58th Annual Forum, Montreal, Canada, June 2002.

16. McKenzie, R.L., and Reinath, M.S., "Planar Doppler Velocimetry Capabilities at Low Speed and Its Application to a Full-Scale Rotor Flow," Paper AIAA 2000-2292, 21st AIAA Aerodynamic Measurement Technology and Ground Testing Conference, Denver, CO, June 2000.

17. Yeo, H., and Shinoda, P. M., "Investigation of Rotor Loads and Vibration at Transition Speed," American Helicopter Society 58th Annual Forum, Montreal, Canada, June 2002.

18. Johnson, W., "Rotorcraft Aerodynamics Models for a Comprehensive Analysis," American Helicopter Society 54th Annual Forum, Washington, D.C., May 1998.

19. McKenzie, R.L., "The Application of Planar Doppler Velocimetry to the Intra-Blade Wakes of a Full-Scale Rotor Flowfield," NASA Contract PO A55156D (NCV) Final Report, November 2001.